Applied Catalysis B: Environment and Energy 399 (2026) 127073

Contents lists available at ScienceDirect

Applied Catalysis B: Environment and Energy

journal homepage: www.elsevier.com/locate/apcatb

Performance enhancement of Pd-based selective ammonia oxidation catalysts through forced dynamic operation

Thomas Häber [a,*], Camilo Cárdenas [b], Sreelakshmi Vijayaraghavan [b], Iadh Ben Othman [b], Anna Zimina [a], Florian Maurer [b], Jan-Dierk Grunwaldt [a,b], Olaf Deutschmann [a,b], Patrick Lott [b,*]

[a] Institute of Catalysis Research and Technology, Karlsruhe Institute of Technology (KIT), Hermann-von-Helmholtz-Platz 1, Eggenstein-Leopoldshafen, 76344, Germany

[b] Institute for Chemical Technology and Polymer Chemistry, Karlsruhe Institute of Technology (KIT), Engesserstr. 20, Karlsruhe, 76131, Germany

ARTICLE INFO

Dataset link: https://doi.org/10.35097/n63tnnpyt3mmt10b

Keywords:
Emission control
Forced dynamic operation (FDO)
Palladium catalyst
Selective ammonia oxidation (SCO)
Spatial profiling (SpaciPro)

ABSTRACT

In light of the increasing relevance of alternative energy carriers, the established domain of emission control is confronted with novel challenges. Among these carriers, ammonia (NH_3) has emerged as particularly promising due to its high energy density and carbon-free nature. This study focuses on the selective catalytic oxidation (SCO) of NH_3 to elemental nitrogen (N_2) under lean conditions. While conventional platinum-based catalysts exhibit high activity, they suffer from poor N_2 selectivity and significant formation of nitrous oxide (N_2O), a potent greenhouse gas. As an alternative, palladium-based catalysts are investigated due to their inherently higher selectivity toward N_2. Although palladium exhibits limited activity under static feed conditions, its performance is markedly enhanced under forced dynamic operation (FDO), wherein short, intermittent reducing pulses are introduced through oxygen cut-off. This operational mode not only boosts catalytic activity beyond that of platinum but also preserves palladium's superior selectivity. *Operando* time-resolved X-ray absorption spectroscopy (XAS) and *ex situ* Raman spectroscopic analysis of spent catalyst samples indicate that FDO promotes the formation of metallic palladium, which exhibits higher activity compared to palladium oxide that is the predominant phase under lean conditions. *Operando* XAS uncovers that a finite fraction of metallic palladium is retained at the catalyst inlet, enhancing low-temperature activity and likely contributing to improved long-term stability as long as 300 °C is not exceeded for extended periods. These findings correspond directly to axially resolved concentration profiles of gas phase species, which reveal the development of a highly active front zone during FDO, where the majority of NH_3 conversion occurs selectively to N_2. This phenomenon is observed under both dry and humid conditions, underscoring the robustness of the approach. The results suggest that FDO enables the use of significantly shorter monolithic converters for selective NH_3 oxidation, i.e., a reduction of length by up to 50% in realistic humid conditions, thereby offering substantial reductions in both reactor volume and noble metal demand for practical applications.

1. Introduction

With the growing relevance of alternative energy carriers, conventional emission control strategies are increasingly challenged by changes in boundary conditions and progressively stringent emission regulations. Among these carriers, ammonia (NH_3) stands out due to its high energy density, carbon-free nature, and the existence of a globally established infrastructure for large-scale production, transportation, and storage [1,2]. Compared to liquid hydrogen (H_2), NH_3 is more economically liquefied and possesses a higher volumetric energy density, making it a promising hydrogen carrier. Upon decomposition, NH_3 yields H_2 and elemental nitrogen (N_2). Furthermore, NH_3 can be directly utilized as a fuel in combustion engines, particularly in large-bore applications such as marine propulsion systems and stationary combined heat and power plants [3,4]. A common challenge across these applications is the incomplete conversion of NH_3, resulting in (trace) emissions. Given the toxicity of NH_3, its release into the environment must be strictly avoided.

Among the various materials investigated for the selective catalytic oxidation (SCO) of NH_3 to N_2 and water (H_2O) under lean conditions, commonly referred to as NH_3-SCO, non-noble metal-based catalysts

* Corresponding authors.
E-mail addresses: thomas.haeber@kit.edu (T. Häber), patrick.lott@kit.edu (P. Lott).

https://doi.org/10.1016/j.apcatb.2026.127073
Received 19 January 2026; Received in revised form 8 May 2026; Accepted 4 June 2026
Available online 20 June 2026

generally exhibit inferior activity compared to their noble metal-based counterparts [5–7]. In general, platinum (Pt) has been identified as exhibiting superior catalytic activity for NH_3-SCO. However, this advantage is diminished by its relatively low selectivity toward the desired product N_2. Conversely, palladium (Pd) demonstrates higher selectivity but lower overall activity. This trade-off becomes particularly evident when comparing simple catalyst formulations: When applying a O_2/NH_3 ratio of 7.2, Gang et al. [8] observed complete NH_3 conversion at 200 °C over Pt/Al_2O_3 with a N_2 selectivity of 87%, whereas Pd/Al_2O_3 requires temperatures up to 300 °C to achieve full NH_3 conversion, albeit with a maximum N_2 selectivity of 98%. High selectivity is critical for the development of efficient NH_3-SCO processes, as oxidation under lean conditions may lead to undesirable byproducts such as nitrogen oxides (NO, NO_2), which are toxic, or nitrous oxide (N_2O), a potent greenhouse gas with a global warming potential (GWP_{100}) of approximately 273 [9]. The use of alternative support materials, in particular zeolites such as ZSM-5, zeolite Y, or chabazite, has demonstrated potential in enhancing both activity and selectivity [8,10–13]. These improvements were attributed to modifications in the reaction mechanism and oxidation state of the noble metal. Nevertheless, the choice of noble metal remains a decisive factor in catalyst performance, rendering the more selective Pd an attractive candidate for further development.

In addition to material innovations, optimization of operating conditions can significantly enhance catalytic performance. In this context, forced dynamic operation (FDO), defined as the externally induced modulation of the reaction environment within chemical reactors, has emerged as a particularly promising approach. A seminal review by Bailey [14] that was published in 1973 highlighted the conceptual foundations of FDO and its potential advantages over conventional steady-state operation, indicating that the strategy has been recognized for several decades. Despite its inherent complexity, FDO was successfully translated into industrial practice during the 1990s [15]. More recently, its application has garnered renewed interest, particularly within the field of heterogeneous catalysis, where dynamic modulation is increasingly being explored as a means to overcome kinetic limitations and improve overall process efficiency [16,17].

Our present work builds on recent advances in the field of emission control, which demonstrated improved methane conversion over lean-operated Pd-based oxidation catalysts via short reducing pulses as a form of FDO [18]. Therein, FDO of monolithic Pd-based oxidation catalysts enables the formation of a highly active zone, whose exceptional performance was traced back to a PdO/Pd mixed phase with particularly active PdO sites that do not suffer from water inhibition due to the continuous removal of hydroxyl groups during the short rich phases. Motivated by the remarkable performance improvement during both light-off and steady-state operation, the present study explores NH_3-SCO over a Pd/Al_2O_3 catalyst operated under lean conditions. Herewith, we aim at employing the unique Pd/PdO-redox chemistry and enforcing axial oxidation state gradients that are advantageous for NH_3-SCO. Beyond the observed activity enhancement through FDO, particular emphasis is placed on product selectivity, which is particularly critical in the context of NH_3 oxidation. End-of-pipe measurements confirm the effectiveness of FDO under both dry model-like and more realistic humid conditions. Complementary *operando* X-ray absorption and spatially resolved *ex situ* Raman spectroscopic characterization and spatial profiling (SpaciPro) experiments reveal the formation of axial gradients along the catalyst bed, which are instrumental in understanding the performance improvements. Our findings suggest that the strategic application of FDO may enable significant reductions in catalyst volume and noble metal loading, offering a promising pathway toward more efficient and sustainable emission control solutions for NH_3-based energy systems.

Table 1
Catalyst properties as determined by elemental analysis (ICP-OES), TEM imaging, and N_2 physisorption.

	Pt/Al_2O_3	Pd/Al_2O_3
Loading	1.88 ± 0.10 wt. − %	2.40 ± 0.12 wt. − %
Nanoparticle size	2.0 ± 0.9 nm	5.8 ± 2.2 nm
Dispersion	56 %	20 %
M_{PGM}	195.1 g/mol	106.4 g/mol
Surface area	136 m^2/g	132 m^2/g
Average pore diameter	8.5 nm	26.0 nm

2. Experimental

2.1. Materials

The catalyst was prepared using the CATIMPREG platform (Chemspeed) for automated incipient wetness impregnation [19]. A solution of tetraamineplatinum(II) nitrate or tetraaminepalladium(II)nitrate (Fischer Scientific, 99.99 %) diluted in water was added dropwise to a commercial aluminum oxide support ($\gamma-Al_2O_3$, Sasol Puralox TH 100/150, calcined for 5 h at 700 °C in static air). Subsequently, the material was dried for two hours at 75 °C and a reduced pressure of 120 mbar. After drying, these two steps were repeated eight times in total to achieve the desired noble metal loading. The received sample was then calcined for 5 hours at 500 °C in static air. The final metal loading amounted to (1.88 ± 0.10) wt. − % for platinum and (2.40 ± 0.11) wt. − % for palladium as determined by ICP-OES (inductively coupled plasma-optical emission spectrometry). The average particle size of nanoparticles was determined by transmission electron microscopy (TEM) imaging. For this purpose, the samples were deposited onto a copper grid using a dry-mixing procedure, and were acquired at multiple magnifications. The mean particle size of the nanoparticles was determined with the FIJI software package [20] by measuring the longest diameter of at least 500 individual nanoparticles. Dispersion values were calculated under the assumption of ideally hemispherical nanoparticles [21] and were cross-validated by CO chemisorption experiments. Table 1 summarizes the results of the powder catalyst characterization.

2.2. Setups

2.2.1. Channel reactor

The channel reactor has been described in detail in previous work [22] and represents an improved version of the established design for studying planar, supported (emission control) catalysts [23]. It features a channel that is 2 mm high and 20 mm wide, which ensures undisturbed laminar flow and minimal dead volume, which facilitates rapid gas switching and pulsing experiments. The thermally insulated stainless steel body provides sufficient thermal inertia for stable operation during highly exothermic reactions across a wide temperature range. This design enables light-off measurements at heating rates of 2 K/min and temperatures up to 550 °C, while maintaining a uniform temperature field at the sample location with variations of at most 1 °C along the catalyst layer. The channel is formed by replaceable inlays, allowing easy catalyst plate exchange and flexibility in plate and channel dimensions. Heating is provided by four mineral-insulated heating wires (ThermSys GmbH) embedded in the stainless steel casing and controlled by a programmable PID controller (Eurotherm 3208). Thermocouples are positioned near the catalytic layer and throughout the reactor body to monitor temperature distribution.

The sample plate is made from a stainless steel slab (20 mm wide and 50 mm long) that is plasma-coated with an $\alpha-Al_2O_3$ layer, onto which the active catalyst is subsequently applied. The $\alpha-Al_2O_3$ layer functions solely as an inert protective coating and as a support, enabling the actual $Pd/\gamma-Al_2O_3$ catalyst to be deposited on the metal plate with

sufficient mechanical stability. The catalyst layer is built up stepwise from aqueous slurry of the catalyst using an airbrush pistol, with each layer dried at elevated temperature before the next layer is applied. In total, 10 to 15 layers are deposited, resulting in a specific surface noble metal loading of approximately 1 μg/mm^2. The coated plates were calcined at 550 °C for 5 hours. Note that the uniformity of the coatings produced using this method has previously been confirmed by X-ray absorption near-edge structure (XANES) measurements along the catalyst [22]. Gas phase composition at the reactor outlet was analyzed using a Fourier-transform infrared spectrometer (FTIR, MG2030, MKS Instruments).

2.2.2. XAS setup

The chemical state of palladium (Pd, K edge, 24.35 keV) was investigated by X-ray absorption spectroscopy (XAS) at the CAT-ACT beamline of the KIT Light Source (Eggenstein-Leopoldshafen, Germany) [24], using the same channel reactor described in the previous section. This reactor is equipped with 28 μm thick aluminum X-ray windows, which are placed opposite the catalytic plate and define the upper boundary of the 2 mm high catalytic channel [22]. The experiments used a Pt/Rh mirror system and a Si(311) double-crystal monochromator to select the X-ray beam energy. The beam size was adjusted to 3 × 3 mm^2. X-ray absorption spectra were recorded in fluorescence mode using a 4-element solid-state detector (ME4-Vortex, Hitachi High-Tech America, Inc.), with the region of interest centered on the Pd K$\alpha_{1,2}$ emission line. The photon energy was calibrated to the tabulated value of 24.35 keV using the K-edge data of a metallic Pd foil. XANES spectra were recorded between 24.25 keV and 24.75 keV (474 points, 120 s per scan). Throughout all experiments, the gas phase composition at the reactor outlet was continuously monitored using a mass spectrometer (OmniStar, Pfeiffer) in combination with Fourier-transform infrared spectroscopy (FTIR, MG2030, MKS Instruments).

The channel reactor facilitates time- and spatially-resolved XAS measurements under conditions that are identical to those employed in the end-of-pipe screening experiments (i.e., with respect to sample geometry and form, flow profile, operating conditions, and so forth). During light-off and light-out experiments, XANES spectra were collected at a position 5 mm downstream from the inlet edge of the 50 mm long catalytic plate in order to monitor the influence of temperature and reaction conditions on the oxidation state at the location where the most pronounced changes are expected. Note that the X-ray absorption spectra acquisition timing was synchronized to the reducing pulses, which maximizes the relevance of the data with regard to temporal resolution.

At predefined temperatures, the light-off/out profiles were temporarily paused, maintaining the reactor at a constant temperature under inert conditions to "freeze" the catalytic state, thereby enabling additional acquisition of spatially resolved XANES data at 10 mm intervals along the catalyst plate. A comparison of the integral catalytic activity obtained from light-off/out measurements conducted with and without such intermittent temperature holds revealed no differences in catalytic performance. This demonstrates that the interruption of the temperature ramp for *in situ* spatial profiling does not perturb the catalytic state or its performance.

2.2.3. Spatial profiling (SpaciPro) setup

Monolithic catalyst samples were investigated using an advanced experimental setup designed to enable comprehensive gas phase analysis. This system integrates an FTIR analyzer (MG2030, MKS Instruments) for monitoring the outlet gas composition and a quadrupole mass spectrometer (HPR-20, Hiden Analytical) for spatially resolved gas phase profiling. The latter employs the capillary-based spatial profiling (SpaciPro) technique to acquire axial concentration profiles of reactive species within the monolith channels. As detailed in previous studies [25,26], the setup comprises mass flow controllers (MFCs) for precise regulation of gas feed, a quartz glass reactor configured in plug-flow geometry suitable for housing monolithic samples, and a motorized linear translation stage. This stage facilitates the controlled movement of a slender quartz capillary (inner/outer diameter of 100/170 μm) that is connected to the mass spectrometer and positioned within a central channel of the monolith, thereby enabling localized sampling of the gas phase along the reactor axis.

Cordierite monoliths (cell density of 600 cpsi) with a length of 50 mm and a diameter of 18 mm (equal to 222 channels) were prepared by dip-coating in an aqueous slurry of the catalyst powder following the procedure described previously [26]. Similar to the plate preparation, the catalyst was applied in multiple layers, with channels blown clear using compressed air after each step and the monolith dried at approximately 60 °C after each layer. For both catalyst types, the precious metal loading was 80 g/ft^3, corresponding to a surface loading of 1 μg/mm^2, identical to the plates. Considering the differing metal loadings of the Pt/Al_2O_3 and Pd/Al_2O_3 catalysts, along with their respective particle sizes and dispersions (see Table 1), the resulting number of surface sites is similar for both metals; namely 1.54×10^{21} sites/m^2 for Pt/Al_2O_3 and 1.13×10^{21} sites/m^2 for Pd/Al_2O_3. The coated monoliths were subsequently calcined at 550 °C for 5 hours.

2.3. Testing protocol

Regardless of the specific experimental configuration employed, light-off tests were utilized as the primary method for assessing the catalytic performance of the monolithic samples. Initial evaluations were conducted under model conditions comprising 1000 ppm NH_3, 10 vol. – % O_2, and balance N_2. To simulate more realistic operating environments, additional tests were performed under humid conditions representative of practical applications, specifically using a gas mixture of 1000 ppm NH_3, 10 vol. – % O_2, 10 vol. – % H_2O, and balance N_2. Selected temperatures of particular interest — based on observed catalytic behavior — were further investigated through steady-state experiments using both dry and humid gas compositions. For all channel reactor experiments, a temperature ramp rate of 2 K/min and a gas hourly space velocity (GHSV) of 30 000 h^{-1} were applied. In contrast, experiments conducted using the SpaciPro setup employed a ramp rate of 3 K/min and a GHSV of 9500 h^{-1}. Irrespective of the setup configuration, the catalytic tests were conducted in a temperature window ranging from 100 °C to 400 °C. Considering the temperature-dependent species evolution, this is the relevant temperature regime for the Pd-based NH_3-SCO catalyst subject to this study on the one hand; on the other hand, this matches well with typical tailpipe temperatures of lean-operated NH_3 energy conversion applications, such as combustion engines [27,28].

During both light-off and steady-state testing, forced dynamic operation (FDO) was implemented by periodically interrupting the otherwise lean reaction conditions. Specifically, every 60 s, the oxygen feed was suspended for a duration of 10 s, while keeping the overall flow rate constant, thereby inducing transient net-reducing conditions within the reactor. This approach enabled the investigation of catalyst behavior under dynamically fluctuating redox environments.

3. Results and discussion

3.1. Basic performance tests in channel reactor

In the first stage of this study, plates coated with Pt/Al_2O_3 and Pd/Al_2O_3 were subjected to baseline performance tests in a channel reactor using a feed gas mixture comprising 1000 ppm NH_3, 10 vol. – % O_2, and N_2 as balance. The corresponding results are presented in Fig. 1. For the benchmark catalyst Pt/Al_2O_3, NH_3 conversion commences at approximately 150 °C, followed by a pronounced light-off and nearly complete conversion at around 250 °C. N_2 and N_2O concentrations initially increase concurrently, with N_2 reaching a maximum near 230 °C before declining, whereas N_2O continues to rise, attaining a peak concentration of 338 ppm at approximately 270 °C. Further temperature

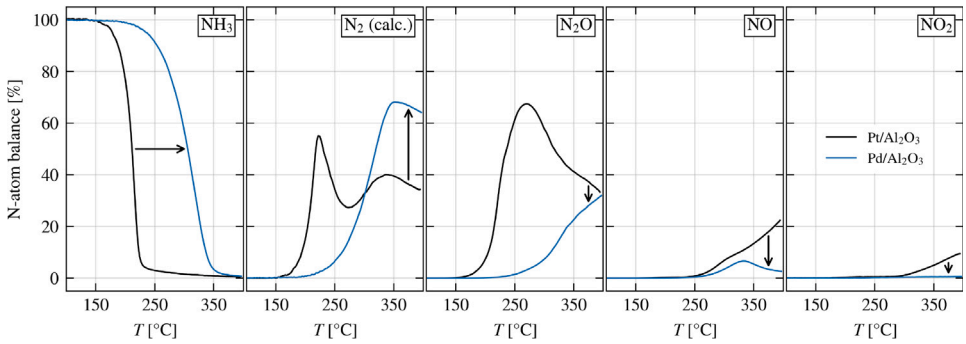

Fig. 1. N-atom balance during light-off over plates coated with Pt/Al_2O_3 (black) and Pd/Al_2O_3 (blue), obtained in the channel reactor, with a time-invariant (constant) inlet feed (1000 ppm NH_3, 10 vol. – % O_2, balance N_2; 2 K/min, GHSV 30 000 h^{-1}).

increase promotes the formation of NO and NO_2, accompanied by a second yet local N_2 maximum at about 330 °C. The predominance of N_2O as a reaction product is particularly concerning due to its strong greenhouse effect, which constitutes the primary motivation for replacing Pt with the more selective Pd in this study.

Compared to Pt/Al_2O_3, Pd/Al_2O_3 exhibits markedly higher selectivity toward the target product N_2, achieving a global maximum of 340 ppm at approximately 350 °C, while generating substantially lower amounts of N_2O and NO. NO_2 formation was negligible. Despite this significantly improved selectivity — in fact, the N_2O/NO ratio over Pd remains consistently lower than that over Pt across the entire temperature range (see SI, Figure S1) — the reduced activity of Pd/Al_2O_3 represents a major limitation, as relevant NH_3 conversion occurs only above 250 °C and complete conversion requires temperatures well above 350 °C. Moreover, the temperature of 50% conversion, T_{50}, is 210 °C over Pt but 305 °C over Pd.

Given the superior catalytic activity of Pt/Al_2O_3, strategies to improve the performance of Pd/Al_2O_3 are essential. In this context, forced dynamic operation (FDO), a reaction engineering approach widely recognized for enhancing catalytic reactor performance [15–17], was implemented. Specifically, short reducing pulses (SRPs) were introduced, defined as interrupting lean operation every 60 s for 10 s by temporarily cutting off the oxygen supply. As illustrated in Fig. 2, SRP operation has negligible influence on overall NH_3 conversion and product selectivity during the initial phase of the first light-off. However, once a threshold temperature of approximately 290 °C is reached, the light-off curves under static and dynamic conditions begin to diverge, indicating catalyst activation induced by pulsing. This activation becomes markedly evident during a second, consecutive light-off experiment: NH_3 conversion initiates well below 150 °C, and T_{50} was determined to be approximately 180 °C, representing a reduction of 125 °C compared to Pd/Al_2O_3 in static operation and of 30 °C compared to the benchmark Pt/Al_2O_3 catalyst. This enhanced light-off behavior under continuous pulses stabilizes after the first cycle and does not change with additional cycling, indicating that the improvement is not caused by processes such as gradual PdO reduction but instead represents a reproducible response to the applied reductive pulsing protocol (see supplementary material for further details).

Apart from a moderate increase in NO formation at elevated temperatures ($T > 200$ °C), this substantial activity enhancement does not compromise the high selectivity of Pd/Al_2O_3. On the contrary, due to the improved catalytic activity, product formation occurs at lower temperatures, with significantly higher N_2 concentrations and markedly reduced N_2O levels under dynamic operation compared to the Pt-based benchmark system. Notably, NO_2 formation remains irrelevant also under dynamic conditions. Furthermore, alternating exposure of the samples to reductive pulses over multiple light-off/light-out cycles (at least four cycles), or complete reduction with hydrogen followed by regeneration under 10 vol. – % oxygen, does not produce any detectable deterioration in the overall catalytic performance. In all cases, the conversion rates were fully reproducible under static lean conditions as well as during operation with reductive pulses, suggesting that alterations in, for example, the particle size distribution that would measurably affect the catalyst's performance are negligible under the reaction conditions applied herein.

While the substantial performance enhancement achieved through FDO is remarkable, the durability of the activated catalyst state remains an open question. To address this, several long-term experiments were conducted under three distinct conditions: (i) dynamic operation, (ii) lean operation following activation via FDO, and (iii) lean operation after prior reduction of the catalyst. A temperature of 230 °C was chosen for these tests because it corresponds to the point where the light-off curves of the benchmark Pt/Al_2O_3 and the FDO-activated Pd/Al_2O_3 catalysts exhibit their maximum N_2 selectivity (compare Figs. 1 and 2), while also ensuring high NH_3 conversion, thus providing conditions relevant for practical applications. Fig. 3 shows the concentration of N_2 and N_2O at the reactor outlet, again expressed as an N-atom balance, over a period of up to 24 h. It is shown once for operation with reductive pulses (blue) and under static conditions (black), after the pulses have been switched off. Beforehand, the sample was activated by four successive light-off/out cycles with continuous SRPs. The enlarged sections illustrate the temporal variation of the outlet concentration during the SRPs. For comparison, the mean value over a full SRP cycle is also shown (open, blue circles), which is very close to the static operation after pulse activation. In addition, data from a long-term measurement on a previously reduced sample are shown (green), which indeed exhibits a higher NH_3 conversion, but also slightly increased N_2O concentrations at the reactor outlet. The data summarized in Fig. 3 indicate that the catalyst exhibits negligible deactivation over time on stream under dynamic conditions, maintaining a high NH_3 conversion of just over 80 %. Although this finding is promising, technical applications typically require predominantly lean operation, for instance in combustion processes where engine efficiency is prioritized. Consequently, dynamic operation may only be feasible intermittently to (re-)activate the catalyst. To simulate such scenarios, SRP operation was terminated and the catalyst was subsequently operated under static lean conditions for an additional 24 h. Remarkably, NH_3 conversion even slightly increased, while N_2O concentrations remained unchanged.

Given the potential complexity of implementing frequent short reducing periods in technical systems, a straightforward pre-reduction strategy was also evaluated, since earlier research suggests feasibility for performance enhancement [10]. Interestingly, the pre-reduced catalyst outperformed the pulse-activated sample in terms of NH_3 conversion; however, this improvement came at the expense of increased N_2O formation. Considering the extremely high global warming potential (GWP_{100}) of N_2O, namely approximately 273 times greater than CO_2 [9], selectivity will likely be prioritized over activity. In such cases, external measures such as electrical heating could be employed to achieve higher conversion without causing elevated N_2O emissions.

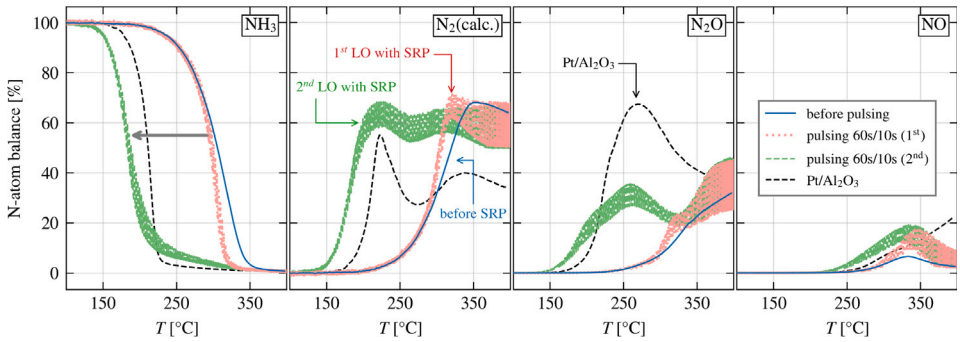

Fig. 2. Effect of continuous, short reductive pulses (SRPs) on the first and second light-off. Activation of Pd/Al_2O_3 occurs in a threshold temperature window around 300 °C. For reference also the light-off curves for Pt/Al_2O_3 and Pd/Al_2O_3 without SRPs are shown. (1000 ppm NH_3, 10 vol. – % O_2 (SRP: 60 s on, 10 s off), balance N_2; 2 K/min, GHSV 30 000 h^{-1}).

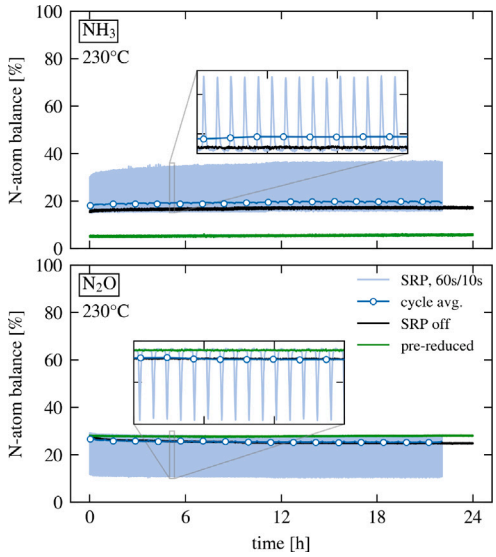

Fig. 3. Stability of the catalytic performance of activated Pd/Al_2O_3 at 230 °C, well below the activation threshold temperature, and for up to 24 h. There is hardly any drop in performance with SRPs, even when pulse operation is switched off (SRP off). NH_3 conversion and N_2O yield for a pre-reduced sample are also provided for reference (see text for details).

It is noteworthy that the pre-reduced catalyst also demonstrated stable performance over 24 h, suggesting a certain robustness of its oxidation state under the conditions investigated herein. The absence of any measurable re-oxidation (i.e., loss of catalytic activity) of the pre-reduced Pd/Al_2O_3 catalyst at 230 °C, even after 24 h in the presence of 10 vol. – % O_2, can be rationalized by the well-established kinetic constraints on the formation of surface PdO at low temperature. While oxygen can adsorb on metallic Pd under these conditions, the transformation to bulk (crystalline) PdO generally proceeds only at temperatures above approximately 250 °C to 300 °C for particle sizes exceeding 5 nm [29–31], which corresponds to the particle size regime investigated in this study. This conclusion is corroborated by our own X-ray absorption spectroscopy (XAS) measurements, which are presented in a subsequent section.

The robustness of the activated catalyst state is further corroborated by continuous and step-wise light-off/light-out experiments (see SI, Figure S3), which demonstrate that the oxidation state and corresponding catalytic performance remain stable for at least 1 h not only at 230 °C, which is the temperature selected for long-term tests, but across a broader range from 175 °C to 400 °C. Taking typical exhaust temperatures of NH_3-fueled applications into account, this observation is encouraging.

3.2. Characterization in spatial resolution

Following exposure to FDO conditions, visual inspection of the catalyst plate showed a clear axial gradient: a dark brown zone with parabolic shape originating at the catalyst inlet, transitioning to light brown toward the rim and outlet, most likely due to the oxidation of metallic Pd (dark brown) to PdO (light brown). To obtain insight into the spatial variation of the oxidation state, spatially resolved *ex situ* Raman spectroscopic mapping was performed at 11 distinct locations on the catalyst plate (see Fig. 4) using 532 nm excitation. For this, an inVia Raman spectrometer (Renishaw) equipped with a frequency doubled Nd:YAG laser (532 nm) and a Leica DM2500 optical microscope was used. Spectra were recorded at 11 different points in the spectral range of 100 cm^{-1} to 1300 cm^{-1}. Data treatment was done using WiRE 4.2 (Renishaw). The spectra were processed by applying a polynomial baseline correction and averaging five scans per measurement spot. Spectra obtained from light brown regions exhibited a characteristic peak at 647 cm^{-1}, which indicates the presence of PdO [29,32]. In contrast, this peak was absent in dark brown areas, suggesting the quasi-exclusive presence of metallic Pd formed via reduction by NH_3. The distinct parabolic gradient observed originates from side-wall effects associated with the unique geometry of the channel reactor employed in this study. Due to the zero-flow velocity at the channel side-walls, NH_3 is almost completely consumed near the edges at the inlet region. Consequently, in the downstream sections adjacent to the side-walls, no NH_3 remains to allow for catalyst reduction. Similarly, as the NH_3 concentration progressively decreases along the axial flow direction, the residual levels near the outlet are insufficient to maintain reduction, resulting in an increasing fraction of PdO. Thus, the parabolic profile directly reflects the interplay between the internal flow velocity distribution and the surface catalytic reactions occurring within the channel.

While the parabolic profile or, more precisely, the light-brown regions of PdO at the lateral edges of the plate are primarily a consequence of the lateral confinement of the flow, a gradient in the oxidation state appears to form along the centerline of the plate, which was presumably induced by the reducing pulses. Samples that were exposed exclusively to static, lean conditions show no visible gradients at all.

3.3. In situ/operando XAS for monitoring oxidation state changes

The *ex situ* Raman spectroscopic measurements from the previous section suggest that the observed increase in activity induced by the reducing pulses, along with the associated shift of the T_{50} temperature, is related to the presence of metallic palladium. However, they do not provide any insight into the effect of the reducing pulses under dynamic operation, particularly as a function of operating parameters such as temperature. For this reason, *operando* and *in situ* XAS measurements

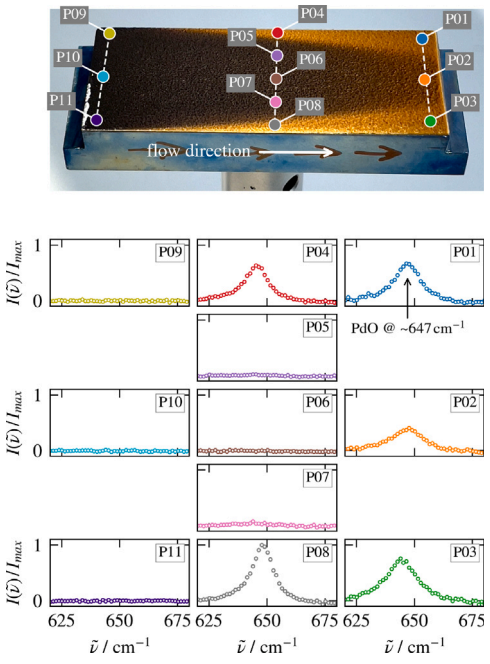

Fig. 4. *Ex situ* Raman spectroscopic mapping uncovering axial oxidation state gradients induced by dynamic pulse operation (see text for details). The typical PdO peak is clearly visible in the lighter areas and is absent in the darker areas, indicating the presence of metallic Pd formed by reduction with NH_3.

were carried out using exactly the same reactor in which the activity tests with and without SRPs described above were performed.

Normalized XANES spectra collected during oxidative (lean) and reductive pre-treatment and averaged over at least 70 scans are used as reference spectra in the subsequent analysis (see Fig. 5). This procedure minimizes systematic errors in the data evaluation that could arise from subtle discrepancies between the spectra of bulk Pd or bulk PdO and those of reduced or oxidized Pd nanoparticles, respectively, which originate from their small particle or cluster size. Normalization of the XANES spectra was carried out using the PyMca software package [33], employing first-order polynomial fits to the pre-edge and post-edge regions. Reference spectra recorded at different positions along the catalyst bed are essentially identical, indicating the absence of spatial gradients after either oxidative or reductive pre-treatment. For illustration, a single sample spectrum is also displayed in Fig. 5 (open symbols), highlighting the signal-to-noise ratio of the XANES data at the chosen time resolution of 2 min per scan. The spectrum is presented together with the corresponding fit (black line) and residuals (filled symbols), obtained from a linear combination analysis (LCA) using the oxidized and reduced reference spectra. The root-mean-square (RMS) deviation of the residuals is ≈ 0.03.

XAS was recorded under three distinct sets of conditions: (i) light-off/out under lean, static reaction conditions (1000 ppm NH_3, 10 vol. – % O_2, balance N_2); (ii) light-off/out under forced dynamic operation involving the periodic and continuous application of short reducing pulses (10 s reducing pulse, followed by 65 s of lean operation); and (iii) light-off under lean, static conditions using a pre-reduced catalyst (reduction in 1000 ppm NH_3, balance N_2, at 450 °C for 90 min). Prior to the XAS measurements, the catalyst was pre-conditioned by several light-off/out cycles under static lean conditions until no further changes in the integral performance were observed, which is typically achieved after two cycles (see Supplementary Information for additional details on the pre-conditioning protocol). A comparison of the catalytic performance obtained in the previously described screening experiments with that measured during the XAS experiments confirmed the reproducibility of the catalytic behavior and activation by short reducing pulses.

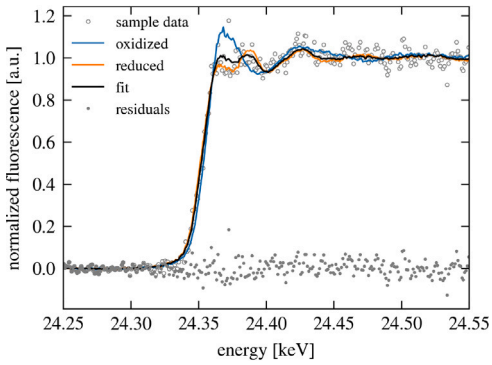

Fig. 5. Pd K-edge XANES reference spectra of metallic Pd and PdO species acquired during oxidative (blue) and reductive (orange) pretreatment of the catalyst (each obtained by averaging at least 70 scans). A typical spectrum measured under reaction conditions is displayed as gray open circles to demonstrate the signal-to-noise ratio, along with its linear-combination fit based on the reference spectra (black line). The corresponding fit residuals are plotted as gray filled circles.

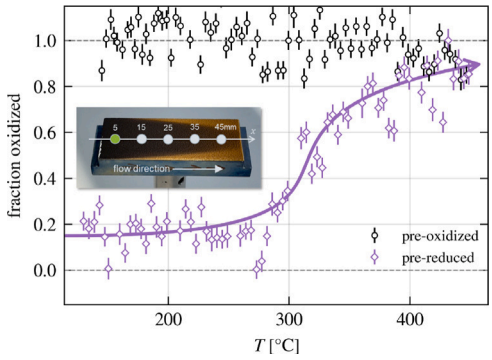

Fig. 6. Variation of the oxidation state near the inlet (x = 5 mm, see inset) as a function of temperature under steady, lean conditions: (a) for a pre-oxidized sample (black circles) and (b) for a pre-reduced sample (purple diamonds). Error bars indicate the 68 % confidence interval derived from the fit of the linear combination of the reference spectra (see text for details). (1000 ppm NH_3, 10 vol. – % O_2, balance N_2; 2 K/min, GHSV 30 000 h^{-1}).

In Fig. 6, the change in the degree of oxidation (fraction of PdO) is shown as a function of temperature under static, lean conditions; once after an oxidative pre-conditioning (black circles) and the other time after the catalyst had previously been reduced (purple diamonds). During the light-off experiments conducted at a heating rate of 2 °C/min, XANES spectra were continuously recorded at a position 5 mm downstream from the inlet edge of the plate (see inset). The temperature associated with the data points corresponds to the mean value during the respective scan. Error bars only represent the error of the fit parameter in the LCA and correspond to the 68 % confidence interval, which is equivalent to the simple standard deviation. The actual uncertainty is reflected in the scatter of the data points, which on average is at ±0.09 (RMS).

After oxidative pre-conditioning, the PdO fraction remains close to 1.0 throughout the entire light-off up to 450 °C, with no evidence of PdO reduction to metallic Pd. *In situ* measurements at various positions along the plate, performed at fixed temperatures between 150 and 450 °C in 50 °C increments under inert conditions (N_2 flow), further confirm that the PdO fraction does not vary along the plate (not shown here). In contrast, for a pre-reduced catalyst the initial PdO fraction is initially about 0.15 and only begins to increase at approximately 280 °C, marking the onset of oxidation in the reaction mixture containing 10 vol. – % oxygen. The purple arrow in Fig. 6 serves merely as a visual

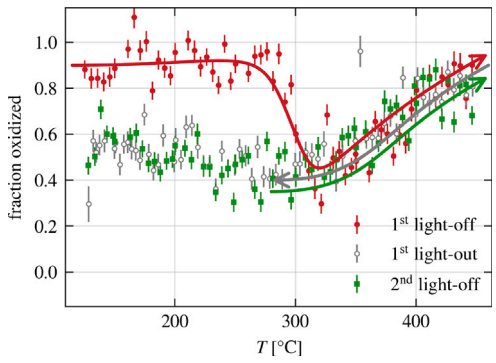

Fig. 7. Impact of continuous, short reducing pulses (SRPs) applied during the first light-off/light-out cycle (red and gray circles, respectively) and the second light-off (green circles) on the fraction of oxidized Pd/Al_2O_3 close to the inlet ($x = 5$ mm, compare Fig. 6). The operating conditions, catalyst pre-treatment, and light-off/light-out protocol are the same as in Fig. 2. Error bars represent the 68 % confidence interval obtained from fitting a linear combination of the reference spectra (see text for further details). (1000 ppm NH_3, 10 vol. – % O_2 (SRP: 65 s on, 10 s off), balance N_2; 2 K/min, GHSV 30 000 h^{-1}).

guide, indicating the direction of the temperature ramp. The fact that the reduced sample does not initially exhibit a PdO fraction close to zero is due to the formation of surface oxides or the interaction with the support that is relevant even under inert conditions. *In situ* spatial profiling under inert conditions shows no oxidation-state gradient during re-oxidation of the reduced sample; instead, the PdO fraction at a given temperature is uniform along the catalyst plate within the measurement uncertainty (see Supplementary Information for details). At 450 °C, the oxidation state matches that of the oxidized catalyst. As mentioned earlier, the light-off performance of the pre-reduced sample is in fact similar to that after FDO, whereas the subsequent light-out again closely resembles that of the oxidized sample, underscoring the reversible character of the oxidation-state and performance changes.

To characterize the influence of short reducing pulses on the oxidation state under dynamic operation, the measurements in Fig. 2 were repeated while monitoring the Pd oxidation state via XAS. While the duration of the reducing pulse remained constant at 10 s, the duration of the lean phase was increased from 60 s to 65 s. In addition, the start of the XANES scans was synchronized with the end of the reducing pulse. In this way, the region around the Pd K edge that is relevant for determining the PdO/Pd ratio remains unaffected by the pulse and reliable probing of the Pd state takes place once the reducing phase was finished. Comparative measurements with a longer lean phase of 140 s, which covers a complete XANES scan, showed no differences, neither with respect to the spectra nor in terms of catalytic performance and activation.

Fig. 7 shows the change of the PdO fraction under FDO during: (1) the very first light-off with SRPs after pre-conditioning (red, filled circles), (2) the subsequent light-out (gray, open circles), and (3) the second light-off (green, filled squares). Again, arrows in Fig. 7 serve as a visual guide and indicate the direction of the temperature ramp. Analogous to the pre-oxidized sample under static lean conditions, the initial light-off with SRPs begins with a PdO fraction close to unity. However, at approximately 280 °C, and in contrast to the behavior observed under static operating conditions, the PdO fraction starts to decrease to about 0.4 at the probed measurement position. This observation demonstrates a pulse-induced reduction of PdO even in the presence of an excess of oxygen. Upon further temperature increase, the PdO fraction rises again in a manner closely resembling the re-oxidation behavior of the pre-reduced sample shown in Fig. 6. The fact that the sample does not reach full oxidation in either case on a time scale shorter than that of the temperature ramp suggests that the oxidation process is comparatively slow relative to the reduction, or that the degree of oxidation is predominantly governed by temperature. The latter interpretation would be consistent with the continuous and step-wise light-off/light-out experiments discussed previously (see SI, Figure S3).

During the subsequent light-out, the oxidation state again decreases to approximately 0.4 upon decreasing the temperature to 300 °C, closely reproducing the oxidation state behavior observed during the initial light-off in this temperature interval. Upon further cooling, however, the PdO fraction remains constant at this low level, consistent with the observation that oxidation to PdO generally requires temperatures above approximately 250 °C to 300 °C for the particle sizes employed in this study [29–31,34]. The second light-off then replicates the preceding light-out with respect to both the degree of oxidation and the catalytic performance. Consequently, under operation with continuous dynamic pulsing, a finite fraction of metallic palladium is retained during cooling, thereby enhancing the catalytic activity at lower temperatures and accounting for the corresponding decrease in T_{50}. In contrast to the static measurements, the *in situ* measurements after pulsing at different positions on the catalytic plate provide clear evidence for the formation of a pulse-induced gradient in the Pd/PdO ratio along the centerline of the plate, in agreement with the *ex situ* Raman spectroscopic measurements. The PdO fraction is only about 40 % to 50 % in the inlet region, while the sample at the end of the plate is still almost fully oxidized. This gradient remains upon cooling under forced dynamic operation, but can be reversibly removed by oxidizing the sample at 450 °C again.

3.4. Translation into realistic monolithic samples and mechanistic interpretation

The channel reactor provides well-defined experimental conditions and enables precise *ex situ*, *in situ*, and even *operando* characterization of the catalytically coated plates, as demonstrated by the XAS measurements presented in the previous section. However, spatial gradients may be particularly pronounced due to the residence time distribution and flow properties in the channel (cf. Häber et al. [22]), where the residence time and the transverse diffusion timescale are of the same order of magnitude. Specifically, the residence time is given by $\tau_{channel} = 1/\mathrm{GSHV} = 120$ ms, and the diffusion timescale in the flat channel ($W \gg H$) can be approximated as $t_{diff} \sim H^2/D \approx 227$ ms [35,36], where $H = 2$ mm and $W = 20$ mm denote the height and width of the channel, respectively, and D is the diffusion coefficient.

It is essential to complement these investigations with tests under more realistic configurations to ensure the transferability of the promising findings discussed above to practical applications. To this end, additional kinetic experiments were performed in a quartz-glass tubular reactor operating under plug-flow conditions, equipped with cylindrical, washcoated honeycomb monoliths of laboratory scale. For the sake of comparability, an identical gas mixture was applied (1000 ppm NH_3, 10 vol. – % O_2, balance N_2), revealing the same trends as observed in the channel reactor when comparing the performance of Pt/Al_2O_3 and Pd/Al_2O_3 (see SI, Figure S5). Due to the small channel size of the 400 cpsi monolith, the transverse diffusion timescale in the nearly cylindrical channels can be estimated as $t_{diff} \sim R^2/(\alpha_1^2 D) \approx 3.3$ ms, where $R \approx 0.58$ mm is the channel radius and $\alpha_1 \approx 2.405$ is the first Bessel eigenvalue [35,36]. Since the transverse diffusion time characterizes how quickly concentration profiles become uniform in the direction perpendicular to the main flow, it follows that the monolithic channels are expected to retain significant axial (streamwise) concentration gradients while exhibiting only minor lateral variations. To promote this behavior, we deliberately selected a GHSV of 9600 h^{-1}, corresponding to a residence time of $\tau_{monolith} = 325$ ms, which lies at the lower bound of values typically employed in practice, thereby reducing lateral concentration gradients in the gas phase to a minimum.

In contrast to the previously employed water-free model gas mixture, additional experiments were performed in which 10 vol. – % of

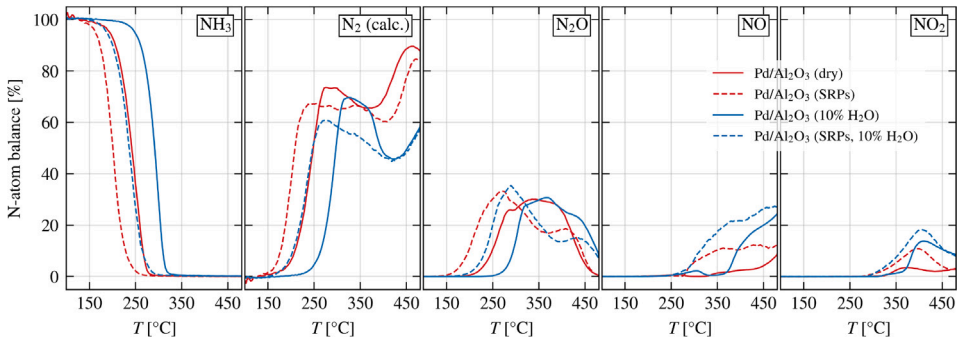

Fig. 8. Effect of SRPs on the performance of a monolithic Pd/Al_2O_3 catalyst under dry and humid conditions. (1000 ppm NH_3, 10 vol. – % O_2 (SRP: 60 s on, 10 s off), 0 or 10 vol. – % H_2O, balance N_2; 3 K/min, GHSV 9600 h^{-1}). Note that, for clarity, the dashed lines represent data obtained during short reducing pulse operation, averaged over an entire 70 s long pulse cycle.

water vapor was introduced to simulate the humidity typically encountered in technical exhaust after-treatment processes. Since water is well known to inhibit catalytic conversion over palladium-based catalyst formulations, particularly in the context of methane oxidation under lean reaction conditions [37–39], investigating the effect of humidity is of particular relevance for the Pd/Al_2O_3 catalyst system. The data presented in Fig. 8 indicate a similar inhibitory effect for ammonia oxidation under lean conditions over Pd. Specifically, the addition of 10 vol. – % water vapor shifts the light-off curve significantly toward higher temperatures, increasing the temperature at 50 % conversion (T_{50}) by 50 °C. In the low-temperature regime (< 275 °C), humidity primarily causes a parallel shift of the selectivity curves toward higher temperatures, whereas at elevated temperatures, it reduces the selectivity toward the desired product N_2. This decrease in selectivity is attributed to overoxidation of NH_3, resulting in increased formation of NO and NO_2.

Given the pronounced water-induced inhibition of selective NH_3 oxidation, mitigating this detrimental effect through forced dynamic reactor operation becomes crucial. As illustrated in Fig. 8, the introduction of short reducing pulses enhances catalytic performance under both dry and humid conditions. In particular, T_{50} decreases by 42 °C and 54 °C in dry and humid environments, respectively, when short reducing pulses are applied. Similar to the observations in the channel reactor experiments (cf. Fig. 2), intermittent oxygen cut-off promotes overoxidation of NH_3, leading to increased NO and NO_2 formation once temperatures exceed 250 °C and 275 °C, respectively. The enhanced formation of NO and NO_2 during dynamic operation can be rationalized by the oxidation state of the noble metal phase. Metallic palladium, whose presence under dynamic conditions is confirmed by Raman and X-ray absorption spectroscopy (cf. Figs. 4 and 7), has been reported to exhibit higher activity for oxidation reactions compared to palladium oxide (PdO) [40–42]. Moreover, the observation of NO_2 formation, in contrast to channel reactor experiments, may be explained by a more intense interaction between the gas phase and the catalytic surface. This is facilitated by the monolithic structure of the catalyst and, more importantly, by the lower space velocity employed. Consequently, space velocity emerges as a critical parameter in the design of full-scale after-treatment systems.

Furthermore, the selectivity toward the most undesired byproduct N_2O requires detailed consideration. Fig. 9 illustrates the amount of N_2O formed during a single light-off experiment as a function of operating conditions, expressed in mmol, specifically for the light-off data shown in Fig. 8. For reference, data for monolith samples washcoated with Pt/Al_2O_3 are shown as well (see Figure S5 in SI for light-off curves). Three key observations can be drawn from Fig. 9. (i) Palladium-based catalyst formulations, regardless of operating conditions, exhibit higher selectivity toward N_2 compared to their platinum-based counterparts. This observation corroborates earlier findings in the literature [8,10], and, considering the strong greenhouse effect of

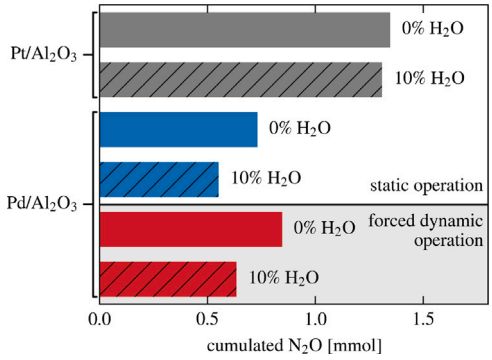

Fig. 9. Cumulated amount of N_2O formed during a single light-off experiment in static lean and forced dynamic SRP operation over Pd/Al_2O_3. Data for the benchmark catalyst Pt/Al_2O_3 are shown as reference. (1000 ppm NH_3, 10 vol. – % O_2 (SRP: 60 s on, 10 s off), balance N_2; 2 K/min, GHSV 9600 h^{-1}).

N_2O, this selectivity advantage justifies the preference for palladium over platinum in ammonia oxidation applications. (ii) Short reducing pulses moderately increase the formation of the undesired secondary emission species N_2O. Thus, the observed activity enhancement enabled by FDO comes at the expense of selectivity. However, given the substantial performance improvement of Pd/Al_2O_3 under FDO (cf. Fig. 8) and the fact that Pd-based formulations remain more selective than Pt-based ones even under dynamic conditions, palladium emerges as a promising candidate for selective ammonia oxidation. (iii) While water vapor inhibits NH_3 activation at least at low temperatures, it simultaneously mitigates N_2O formation. This observation further supports the suitability of palladium-based catalysts for humid ammonia conversion, consistent with prior findings in catalytic wet air oxidation of ammonia, where PdO was identified as one of the most selective catalysts, enabling quasi-exclusive N_2 formation [43].

Although detailed kinetic derivations lie beyond the scope of this study, the performance trends can be interpreted on a mechanistic level in light of existing literature. As mentioned already above, it is well-known that metallic palladium exhibits higher oxidation activity than PdO [40–42]. Furthermore, several studies have addressed the kinetics of NH_3-SCO over Pt in general [44,45] and Pt/Al_2O_3 in particular [46], proposing detailed reaction schemes. According to these models, N_2O formation occurs via the combination of NO* and N* species adsorbed on the Pt surface (* denotes surface adsorbates). Assuming analogous pathways for Pd-based catalysts, a mechanistic hypothesis can be formulated. The higher oxidation potential of (partially) reduced palladium sites leads to more NO_x formation than over PdO, as reflected in the performance data depicted in Fig. 8. The increased NO concentration then facilitates N_2O formation through Pd-mediated NO*

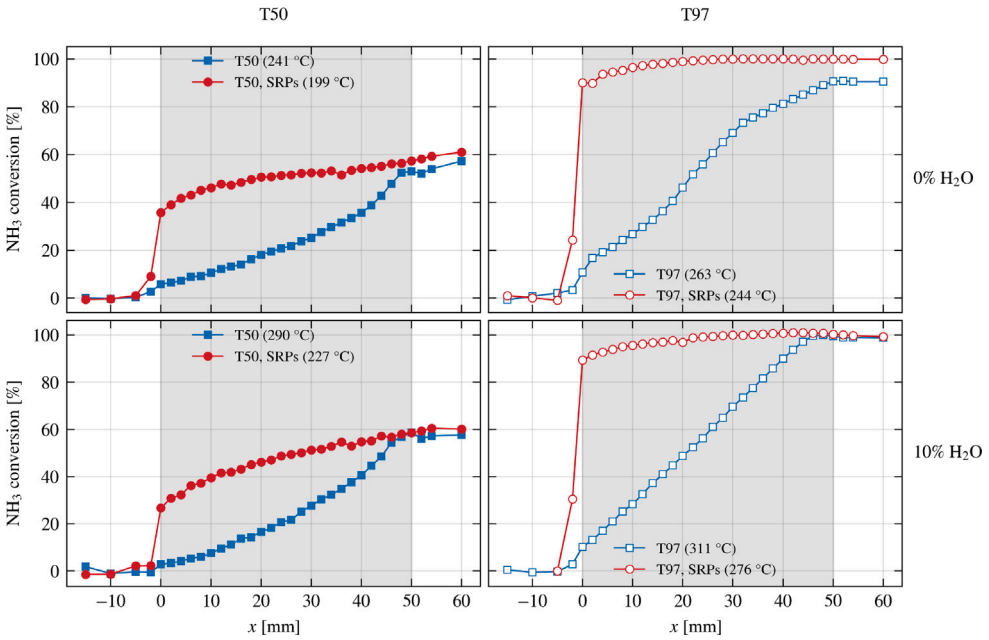

Fig. 10. Axially resolved NH_3 conversion data obtained at T_{50} and T_{97} in time-invariant static conditions and in forced dynamic SRP operation in dry and humid feed. (1000 ppm NH_3, 10 vol. – % O_2 (SRP: 60 s on, 10 s off), 0 vol. – % or 10 vol. – % H_2O, balance N_2; GHSV 9600 h^{-1}).

+ N* combination reactions. Moreover, the kinetic studies suggest the formation of N* proceeds exclusively through one reaction pathway, namely NH_3–S_b + 1.5 O–S_a → N–S_a + 1.5 H_2O + 0.5 S_a + S_b, where S_b denotes an active site for NH_3 storage and S_a represents an active site for all other intermediates. According to Le Chatelier's principle, the presence of water vapor favors the reactant side and thus inhibits the formation of N* species that are a prerequisite for N_2O formation. While this remains a hypothesis, albeit a rational one, it is imperative that future research validates the proposed mechanistic interpretation through comprehensive microkinetic modeling.

3.5. Spatial profiling (SpaciPro)

In the final step, species concentration profiles were obtained via capillary-based spatial profiling, which enables the derivation of NH_3 conversion profiles with axial resolution, as illustrated in Fig. 10. For these experiments, the temperatures corresponding to ~ 50 % and ~ 97 % conversion, as determined during the light-off experiments (Fig. 8), were selected. It is important to note that the absolute end-of-pipe conversion observed during the SpaciPro experiments differs from that in transient operation. This discrepancy arises because the ceramic monolith is thoroughly heated at a constant temperature for an extended period, allowing exothermic heat evolution to fully develop under steady-state conditions. Irrespective of temperature or gas phase conditions, i.e., dry or humid, NH_3 conversion increases steadily along the entire length of the monolith. In clear contrast, profiles obtained under forced dynamic operation, i.e., exposure to short reducing pulses, exhibit a pronounced step near the catalyst inlet, indicating a significant activity enhancement in the front zone. This effect is particularly evident at T_{97}, where more than 90 % of NH_3 is converted within the first few millimeters, followed by a relatively flat profile downstream of the inlet region.

On a fundamental level, the abrupt increase in NH_3 conversion near the inlet, revealed by *in situ* spatial profiling, correlates with a distinct color gradient observed *ex situ* after forced dynamic operation: a dark brown to blackish zone confined to the first few millimeters, while the remainder of the catalyst exhibits a lighter brown hue (see Figure S6 in the SI). Under consideration of the Raman spectroscopy data discussed above (cf. Fig. 4), this color gradient indicates that short reducing pulses generate a front zone dominated by reduced palladium species. In contrast, the majority of the monolith remains in an oxidized state, with Pd^{2+} from PdO as the prevailing electronic noble metal state. The coincidence of higher catalytic activity with metallic palladium in the inlet region aligns with earlier findings by Li and Armor [10], who reported a dramatic increase in low-temperature activity upon reducing PdO/Al_2O_3 catalysts.

The axially resolved profiles are highly relevant also for potential practical implementation. Under static lean conditions, the entire monolith length is required to achieve the desired end-of-pipe conversion. Conversely, forced dynamic operation not only achieves comparable conversion at significantly lower temperatures, e.g., T_{97} = 311 °C for static versus 276 °C for dynamic humid conditions, but also enables near-target conversion within a fraction of the monolith length. This improvement suggests the potential for substantial downsizing of catalytic converters.

Given that cylindrical monolithic geometries, as employed in the SpaciPro experiments herein, are commonly used in technical applications (albeit with larger dimensions), a first-order estimate allows to assume similar performance gains at scale. Based on the profiles at T_{97} (Fig. 10), a size reduction of approximately 60 % could be possible under dry conditions; these may be particularly relevant for ammonia decomposition after-treatment systems where humidity is negligible. A length reduction of about 50 % is possible under humid conditions, which are relevant in emission control of lean-burn ammonia combustion engines. Notably, such downsizing would significantly reduce noble metal demand simply by leveraging more efficient utilization through rational dynamic catalyst operation strategies.

4. Conclusions

With the aim to outperform a conventional Pt/Al_2O_3 catalyst in selective ammonia oxidation, Pd/Al_2O_3 was subjected to forced dynamic operation. Initial experiments employed washcoated plates within a channel reactor. In time-invariant lean gas streams, palladium exhibited lower activity yet significantly higher selectivity toward N_2 compared to platinum. However, the introduction of intermittent short reducing phases that were implemented as a form of forced dynamic operation resulted in a substantial activity enhancement. Once the

light-off temperature under dynamic conditions exceeded a critical threshold, which was determined to be around 280 °C according to *operando* XAS measurements, the catalyst transitioned into an activated state, outperforming platinum in both activity and selectivity across the relevant temperature range. *Ex situ* Raman spectroscopy revealed that oxidized PdO dominated after lean operation, whereas metallic Pd prevailed following dynamic operation. Long-term stability tests (24 h) demonstrated that the activated catalyst state, associated with at least partial palladium reduction, persisted not only under continuous dynamic conditions but also during subsequent lean operation. Furthermore, *operando* XAS experiments performed at the inlet of the catalyst-coated plate reveal that a finite fraction of metallic palladium is preserved during cooling under SRP operation, which enhances catalytic activity at lower temperatures. This behavior may also contribute to the improved long-term stability in the absence of SRPs, as long as temperatures are insufficient to ensure significant re-oxidation.

Subsequent investigations utilized washcoated monolithic honeycomb substrates under both dry and humid conditions. Water vapor inhibited ammonia activation, shifting the light-off toward higher temperatures. Nevertheless, dynamic operation via short reducing pulses effectively activated Pd-based catalysts and mitigated water-induced inhibition. The cumulated amount of N_2O, the most detrimental byproduct, increased only moderately under dynamic conditions and remained substantially lower than that observed for the Pt-based benchmark catalyst. Furthermore, water vapor suppressed N_2O formation, which, based on kinetic considerations, may result from altered surface adsorbate dynamics. Capillary-based spatial profiling provided direct *in situ* insights into monolithic substrates, revealing a steep ammonia conversion gradient near the inlet, followed by moderate conversion downstream. These zones of differential activity correlated with visible color gradients and, in light of Raman spectroscopic and *operando* XAS data, suggested an oxidation-state gradient: highly active yet less selective metallic Pd near the inlet and less active but more selective PdO in the remaining monolith.

Overall, compared to time-invariant lean conditions, forced dynamic operation enables efficient pollutant conversion at significantly lower temperatures. The possibility of operating the catalyst with high activity and high N_2 selectivity over a broader temperature range offers opportunities for direct implementation of the laboratory-scale findings in real-world applications. Furthermore, the pronounced activity boost in the front zone, as revealed by spatial profiling, allows for a reduction in catalyst length by up to 50% under realistic humid conditions. This reduction in catalyst dimensions that is achieved by exploiting palladium sites more effectively through dynamic operation offers a promising strategy to decrease noble metal demand, thereby contributing to environmentally sustainable catalysis twofold, namely through enhanced emission control and reduced reliance on scarce resources.

Future studies should further substantiate the atomic-level insights elucidated herein, preferentially enabled through advanced *in situ* and *operando* techniques that correlate electronic state, surface species, and catalytic performance. Equally important, a systematic alteration of lean-rich cycling periods as well as evaluating potential impact of waveform modulation may unlock additional catalyst performance.

CRediT authorship contribution statement

Thomas Häber: Conceptualization, Data curation, Formal analysis, Investigation, Methodology, Validation, Visualization, Writing – original draft. **Camilo Cárdenas:** Data curation, Formal analysis, Investigation. **Sreelakshmi Vijayaraghavan:** Formal analysis, Investigation, Writing – original draft. **Iadh Ben Othman:** Investigation, Validation. **Anna Zimina:** Investigation, Validation, Writing – review & editing. **Florian Maurer:** Conceptualization, Formal analysis, Investigation, Methodology, Validation, Writing – review & editing. **Jan-Dierk Grunwaldt:** Conceptualization, Funding acquisition, Project administration, Resources, Supervision, Writing – review & editing. **Olaf Deutschmann:** Funding acquisition, Project administration, Resources, Supervision. **Patrick Lott:** Conceptualization, Data curation, Formal analysis, Funding acquisition, Project administration, Supervision, Validation, Writing – original draft.

Declaration of competing interest

The authors declare that they have no known competing financial interests or personal relationships that could have appeared to influence the work reported in this paper.

Acknowledgments

J. Czechowsky is gratefully acknowledged for provision of catalyst powder along with the characterization data and material properties. We would also like to thank T. B. Cataldo and S. Struzek for their assistance with the XAS measurements, and M. Kurt for her support with the Raman spectroscopic measurements. This work was funded by the Deutsche Forschungsgemeinschaft (DFG, German Research Foundation) – SFB 1441 – Project-ID 426888090. Also, DFG is acknowledged for financing the Raman spectrometer (INST 121384/73-1) used in this study. This work was performed with the help of the Large-Scale Data Facility (LSDF) at the Karlsruhe Institute of Technology funded by the Ministry of Science, Research and the Arts Baden-Württemberg and by the Federal Ministry of Research, Technology and Space Germany. Graphics were prepared with the help of the Matplotlib Python package [47].

Appendix A. Supplementary data

Supplementary material related to this article can be found online at https://doi.org/10.1016/j.apcatb.2026.127073.

Data availability

The data that support the findings of this study are available in KITopen at https://doi.org/10.35097/n63tnnpyt3mmt10b.

References

[1] C.W. Ong, N. Chang, M.-L. Tsai, C.-L. Chen, Decarbonizing the energy supply chain: Ammonia as an energy carrier for renewable power systems, Fuel 360 (2024) 130627, http://dx.doi.org/10.1016/j.fuel.2023.130627.

[2] Z. Wen, B. Huang, Y. Wang, K. Wang, X. Tu, P. Xie, X. Fu, Ammonia as a renewable energy carrier from synthesis to utilization, Nat. Rev. Clean Technol. 1 (2025) 755–770, http://dx.doi.org/10.1038/s44359-025-00102-9.

[3] M.-C. Chiong, C.T. Chong, J.-H. Ng, S. Mashruk, W.W.F. Chong, N.A. Samiran, G.R. Mong, A. Valera-Medina, Advancements of combustion technologies in the ammonia-fuelled engines, Energy Convers. Manage. 244 (2021) 114460, http://dx.doi.org/10.1016/j.enconman.2021.114460.

[4] C. Tornatore, L. Marchitto, P. Sabia, M. De Joannon, Ammonia as Green Fuel in Internal Combustion Engines: State-of-the-Art and Future Perspectives, Front. Mech. Eng. 8 (2022) 944201, http://dx.doi.org/10.3389/fmech.2022.944201.

[5] L. Chmielarz, M. Jabł ońska, Advances in selective catalytic oxidation of ammonia to dinitrogen: a review, RSC Adv. 5 (2015) 43408–43431, http://dx.doi.org/10.1039/C5RA03218K.

[6] T. Lan, Y. Zhao, J. Deng, J. Zhang, L. Shi, D. Zhang, Selective catalytic oxidation of NH_3 over noble metal-based catalysts: state of the art and future prospects, Catal. Sci. Technol. 10 (2020) 5792–5810, http://dx.doi.org/10.1039/D0CY01137A.

[7] J. Zhou, B. Guan, J. Guo, C. Zheng, T. Su, J. Chen, Y. Zhang, Y. Yuan, H. Dang, Y. He, Z. Wei, B. Xu, C. Xu, C. Yi, W. Zeng, Z. Huang, Review of the Catalytic System, Synthetic Process, and Support Morphological Research in Selective Catalytic Oxidation of Ammonia, Ind. Eng. Chem. Res. 62 (48) (2023) 20506–20546, http://dx.doi.org/10.1021/acs.iecr.3c02701.

[8] L. Gang, B. Anderson, J. van Grondelle, R. van Santen, NH_3 oxidation to nitrogen and water at low temperatures using supported transition metal catalysts, Catal. Today 61 (1) (2000) 179–185, http://dx.doi.org/10.1016/S0920-5861(00)00375-8.

[9] P. Forster, T. Storelvmo, K. Armour, W. Collins, J.-L. Dufresne, D. Frame, D. Lunt, T. Mauritsen, M. Palmer, M. Watanabe, M. Wild, H. Zhang, The earth's energy budget, climate feedbacks, and climate sensitivity, in: V. Masson-Delmotte, P. Zhai, A. Pirani, S. Connors, C. Péan, S. Berger, N. Caud, Y. Chen, L. Goldfarb, M. Gomis, M. Huang, K. Leitzell, E. Lonnoy, J. Matthews, T. Maycock, T. Waterfield, O.Y. ci, R. Yu, B. Zhou (Eds.), Climate Change 2021: The Physical Science Basis. Contribution of Working Group I To the Sixth Assessment Report of the Intergovernmental Panel on Climate Change, Cambridge University Press, 2021, pp. 923–1054, http://dx.doi.org/10.1017/9781009157896.009.

[10] Y. Li, J.N. Armor, Selective NH_3 oxidation to N_2 in a wet stream, Appl. Catal. B: Env. 13 (2) (1997) 131–139, http://dx.doi.org/10.1016/S0926-3373(96)00098-7.

[11] M. Jabłońska, A. Król, E. Kukulska-Zajac, K. Tarach, L. Chmielarz, K. Góra-Marek, Zeolite Y modified with palladium as effective catalyst for selective catalytic oxidation of ammonia to nitrogen, J. Catal. 316 (2014) 36–46, http://dx.doi.org/10.1016/j.jcat.2014.04.022.

[12] V. Marchuk, X. Huang, J.-D. Grunwaldt, D.E. Doronkin, Structure sensitivity of alumina- and zeolite-supported platinum ammonia slip catalysts, Catal. Sci. Technol. 13 (2023) 2946–2965, http://dx.doi.org/10.1039/D2CY02095E.

[13] D. Kim, S. Xie, K. Ye, X. Zhang, M.T. Caudle, L. Ma, S.N. Ehrlich, F. Liu, Unveiling the support effect in Pt-based catalysts for the selective catalytic oxidation of NH_3 under realistic diesel engine conditions, Catal. Sci. Technol. 15 (2025) 5816–5826, http://dx.doi.org/10.1039/D5CY00681C.

[14] J.E. Bailey, PERIODIC OPERATION OF CHEMICAL REACTORS: A REVIEW, Chem. Eng. Commun. 1 (3) (1974) 111–124, http://dx.doi.org/10.1080/00986447408960421.

[15] P. Silveston, R.R. Hudgins, A. Renken, Periodic operation of catalytic reactors—introduction and overview, Catal. Today 25 (2) (1995) 91–112, http://dx.doi.org/10.1016/0920-5861(95)00101-K.

[16] M. Shetty, A. Walton, S.R. Gathmann, M.A. Ardagh, J. Gopeesingh, J. Resasco, T. Birol, Q. Zhang, M. Tsapatsis, D.G. Vlachos, P. Christopher, C.D. Frisbie, O.A. Abdelrahman, P.J. Dauenhauer, The Catalytic Mechanics of Dynamic Surfaces: Stimulating Methods for Promoting Catalytic Resonance, ACS Catal. 10 (21) (2020) 12666–12695, http://dx.doi.org/10.1021/acscatal.0c03336.

[17] S. Chavez, B. Werghi, K.M. Sanroman Gutierrez, R. Chen, S. Lall, M. Cargnello, Studying, Promoting, Exploiting, and Predicting Catalyst Dynamics: the Next Frontier in Heterogeneous Catalysis, J. Phys. Chem. C 127 (5) (2023) 2127–2146, http://dx.doi.org/10.1021/acs.jpcc.2c06519.

[18] K. Keller, D. Hodonj, L. Zeh, L. Caulfield, E. Sauter, C. Wöll, O. Deutschmann, P. Lott, Spatiotemporal insights into forced dynamic reactor operation for fast light-off of Pd-based methane oxidation catalysts, Catal. Sci. Technol. 14 (2024) 4142–4153, http://dx.doi.org/10.1039/D4CY00625A.

[19] W. Kleist, J.-D. Grunwaldt, High Output Catalyst Development in Heterogeneous Gas Phase Catalysis, in: A. Hagemeyer, A.F. Volpe (Eds.), Modern Applications of High Throughput R&D in Heterogeneous Catalysis, Bentham Science Publisher, 2014, pp. 357–371, http://dx.doi.org/10.2174/9781608058723114010018.

[20] J. Schindelin, I. Arganda-Carreras, E. Frise, V. Kaynig, M. Longair, T. Pietzsch, S. Preibisch, C. Rueden, S. Saalfeld, B. Schmid, J.-Y. Tinevez, D.J. White, V. Hartenstein, K. Eliceiri, P. Tomancak, A. Cardona, Fiji: An open-source platform for biological-image analysis, Nat. Methods 9 (7) (2012) 676–682, http://dx.doi.org/10.1038/nmeth.2019.

[21] G. Bergeret, P. Gallezot, Particle Size and Dispersion Measurements, in: G. Ertl, H. Knözinger, F. Schüth, J. Weitkamp (Eds.), Handbook of Heterogeneous Catalysis, John Wiley & Sons, Ltd, 2008, pp. 738–765, http://dx.doi.org/10.1002/9783527610044.hetcat0038.

[22] T. Häber, S. Wan, S. Struzek, C. Cárdenas, A. Zimina, F. Maurer, P. Lott, R. Suntz, J.-D. Grunwaldt, O. Deutschmann, Novel advanced channel reactor for spatio-temporal activity and catalyst state correlations applied for the reduction of NO by CO over Pt/Al_2O_3, Appl. Catal. A: Gen. 712 (2026) 120748, http://dx.doi.org/10.1016/j.apcata.2025.120748.

[23] A. Zellner, R. Suntz, O. Deutschmann, Two-Dimensional Spatial Resolution of Concentration Profiles in Catalytic Reactors by Planar Laser-Induced Fluorescence: NO Reduction over Diesel Oxidation Catalysts, Angew. Chem. Int. Ed. 54 (9) (2015) 2653–2655, http://dx.doi.org/10.1002/anie.201410324.

[24] A. Zimina, K. Dardenne, M.A. Denecke, D.E. Doronkin, E. Huttel, H. Lichtenberg, S. Mangold, T. Pruessmann, J. Rothe, T. Spangenberg, R. Steininger, T. Vitova, H. Geckeis, J.-D. Grunwaldt, CAT-ACT—A new highly versatile x-ray spectroscopy beamline for catalysis and radionuclide science at the KIT synchrotron light facility ANKA, Rev. Sci. Instrum. 88 (11) (2017) 113113, http://dx.doi.org/10.1063/1.4999928.

[25] C. Diehm, O. Deutschmann, Hydrogen production by catalytic partial oxidation of methane over staged Pd/Rh coated monoliths: Spatially resolved concentration and temperature profiles, Int. J. Hydrog. Energy 39 (31) (2014) 17998–18004, http://dx.doi.org/10.1016/j.ijhydene.2014.06.094.

[26] K.A. Karinshak, P. Lott, M.P. Harold, O. Deutschmann, *In situ* Activation of Bimetallic Pd–Pt Methane Oxidation Catalysts, ChemCatChem 12 (14) (2020) 3712–3720, http://dx.doi.org/10.1002/cctc.202000603.

[27] L. Luo, Z. Huang, Y. Xu, S. Zou, B. Wu, Experimental study on the effect of ammonia on combustion and emission characteristics of a spark ignition engine fueled with hydrogen, ACS Omega 9 (46) (2024) 46339–46348, http://dx.doi.org/10.1021/acsomega.4c07315.

[28] S.A. Reggeti, W.F. Northrop, Lean ammonia-fueled engine operation enabled by hydrogen-assisted turbulent jet ignition, Front. Mech. Eng. 10 (2024) 1368717, http://dx.doi.org/10.3389/fmech.2024.1368717.

[29] A. Baylet, P. Marécot, D. Duprez, P. Castellazzi, G. Groppi, P. Forzatti, In situ Raman and in situXRD analysis of PdO reduction and Pd° oxidation supported on γ-Al_2O_3 catalyst under different atmospheres, Phys. Chem. Chem. Phys. 13 (10) (2011) 4607–4613, http://dx.doi.org/10.1039/C0CP01331E.

[30] K. Zorn, S. Giorgio, E. Halwax, C.R. Henry, H. Grönbeck, G. Rupprechter, CO oxidation on technological Pd-Al_2O_3 catalysts: Oxidation state and activity, J. Phys. Chem. C 115 (4) (2011) 1103–1111, http://dx.doi.org/10.1021/jp106235x.

[31] O. Mihai, G. Smedler, U. Nylén, M. Olofsson, L. Olsson, The effect of water on methane oxidation over Pd/Al_2O_3 under lean, stoichiometric and rich conditions, Catal. Sci. Technol. 7 (14) (2017) 3084–3096, http://dx.doi.org/10.1039/C6CY02329K.

[32] J.-D. Grunwaldt, N. van Vegten, A. Baiker, W. van Beek, Insight into the structure of Pd/ZrO_2 during the total oxidation of methane using combined in situ XRD, X-ray absorption and Raman spectroscopy, J. Phys.: Conf. Ser. 190 (1) (2009) 012160, http://dx.doi.org/10.1088/1742-6596/190/1/012160.

[33] V.A. Solé, E. Papillon, M. Cotte, P. Walter, J. Susini, A multiplatform code for the analysis of energy-dispersive X-ray fluorescence spectra, Spectrochim. Acta, Part B 62 (1) (2007) 63–68, http://dx.doi.org/10.1016/j.sab.2006.12.002.

[34] J.-D. Grunwaldt, B. Kimmerle, S. Hannemann, A. Baiker, P. Boye, C.G. Schroer, Parallel structural screening of solid materials, J. Mater. Chem. 17 (2007) 2603–2606, http://dx.doi.org/10.1039/B705334G.

[35] J. Crank, J. Crank, The Mathematics of Diffusion, second ed., vol. 2, Oxford University Press, Oxford, New York, 1979, 2 edition.

[36] R.B. Bird, W.E. Stewart, E.N. Lightfoot, Transport Phenomena, Wiley, New York, 2007, Revised ed..

[37] K. Persson, L.D. Pfefferle, W. Schwartz, A. Ersson, S.G.J. as, Stability of palladium-based catalysts during catalytic combustion of methane: The influence of water, Appl. Catal. B: Env. 74 (3) (2007) 242–250, http://dx.doi.org/10.1016/j.apcatb.2007.02.015.

[38] P. Velin, M. Ek, M. Skoglundh, A. Schaefer, A. Raj, D. Thompsett, G. Smedler, P.-A. Carlsson, Water Inhibition in Methane Oxidation over Alumina Supported Palladium Catalysts, J. Phys. Chem. C 123 (42) (2019) 25724–25737, http://dx.doi.org/10.1021/acs.jpcc.9b07606.

[39] K. Keller, P. Lott, S. Tischer, M. Casapu, J.-D. Grunwaldt, O. Deutschmann, Methane Oxidation over PdO: Towards a Better Understanding of the Influence of the Support Material, ChemCatChem 15 (11) (2023) e202300366, http://dx.doi.org/10.1002/cctc.202300366.

[40] G.K. Reddy, C. Ling, T.C. Peck, H. Jia, Understanding the chemical state of palladium during the direct NO decomposition – influence of pretreatment environment and reaction temperature, RSC Adv. 7 (2017) 19645–19655, http://dx.doi.org/10.1039/C7RA00836H.

[41] A. Buzková Arvajová, P. Boutikos, R. Pečinka, P. Kočí, Global kinetic model of NO oxidation on Pd/γ-Al_2O_3 catalyst including PdO_x formation and reduction by CO and C_3H_6, Appl. Catal. B: Env. 260 (2020) 118141, http://dx.doi.org/10.1016/j.apcatb.2019.118141.

[42] J. Schütz, H. Störmer, P. Lott, O. Deutschmann, Effects of hydrothermal aging on CO and NO oxidation activity over monometallic and bimetallic Pt-Pd catalysts, Catalysts 11 (3) (2021) 300, http://dx.doi.org/10.3390/catal11030300.

[43] J. Qin, K. Aika, Catalytic wet air oxidation of ammonia over alumina supported metals, Appl. Catal. B: Env. 16 (3) (1998) 261–268, http://dx.doi.org/10.1016/S0926-3373(97)00082-9.

[44] A. Scheuer, W. Hauptmann, A. Drochner, J. Gieshoff, H. Vogel, M. Votsmeier, Dual layer automotive ammonia oxidation catalysts: Experiments and computer simulation, Appl. Catal. B: Env. 111–112 (2012) 445–455, http://dx.doi.org/10.1016/j.apcatb.2011.10.032.

[45] P.S. Dhillon, M.P. Harold, D. Wang, A. Kumar, S.Y. Joshi, Modeling and analysis of transport and reaction in washcoated monoliths: Cu-SSZ-13 SCR and dual-layer Cu-SSZ-13 + Pt/Al_2O_3 ASC, React. Chem. Eng. 4 (2019) 1103–1115, http://dx.doi.org/10.1039/C8RE00325D.

[46] D. Yao, Y. Li, F. Wu, W. Jin, Z. Zhang, X. Hu, J. Hu, Modeling and analysis of ammonia oxidation and nitrous oxide formation on a dual-layer ammonia slip catalyst for diesel after-treatment, React. Chem. Eng. 8 (2023) 2040–2051, http://dx.doi.org/10.1039/D3RE00075C.

[47] J.D. Hunter, Matplotlib: A 2D Graphics Environment, Comput. Sci. Eng. 9 (3) (2007) 90–95, http://dx.doi.org/10.1109/MCSE.2007.55.